

Structure–Property Relationships in Lithium, Silver, and Cesium
Uranyl BoratesShuao Wang,[†] Evgeny V. Alekseev,^{*,†,‡} Jared T. Stritzinger,[†] Guokui Liu,[§] Wulf Depmeier,[‡]
and Thomas E. Albrecht-Schmitt^{*,†}[†]Department of Civil Engineering and Geological Sciences and Department of Chemistry and Biochemistry,
156 Fitzpatrick Hall, University of Notre Dame, Notre Dame, Indiana 46556, United States, [‡]Institut für
Geowissenschaften, Universität zu Kiel, 24118 Kiel, Germany, and [§]Chemical Sciences and Engineering
Division, Heavy Elements and Separation Science, Argonne National Laboratory, Argonne, Illinois 60439,
United States

Received August 4, 2010. Revised Manuscript Received September 27, 2010

Four new uranyl borates, $\text{Li}[(\text{UO}_2)_2\text{B}_5\text{O}_9] \cdot \text{H}_2\text{O}$ (**LiUBO-1**), $\text{Ag}[(\text{UO}_2)_2\text{B}_5\text{O}_8(\text{OH})_2]$ (**AgUBO-1**), $\alpha\text{-Cs}[(\text{UO}_2)_2\text{B}_{11}\text{O}_{16}(\text{OH})_6]$ (**CsUBO-1**), and $\beta\text{-Cs}[(\text{UO}_2)_2\text{B}_{11}\text{O}_{16}(\text{OH})_6]$ (**CsUBO-2**) were synthesized via the reaction of uranyl nitrate with a large excess of molten boric acid in the presence of lithium, silver, or cesium nitrate. These compounds share a common structural motif consisting of a linear uranyl, UO_2^{2+} , cation surrounded by BO_3 triangles and BO_4 tetrahedra to create an UO_8 hexagonal bipyramidal environment around uranium. The borate anions bridge between uranyl units to create sheets. Additional BO_3 triangles extend from the polyborate layers, and are directed approximately perpendicular to the sheets. In $\text{Li}[(\text{UO}_2)_2\text{B}_5\text{O}_9] \cdot \text{H}_2\text{O}$, the additional BO_3 triangles connect these sheets together to form a three-dimensional framework structure. $\text{Li}[(\text{UO}_2)_2\text{B}_5\text{O}_9] \cdot \text{H}_2\text{O}$ and $\beta\text{-Cs}[(\text{UO}_2)_2\text{B}_{11}\text{O}_{16}(\text{OH})_6]$ adopt noncentrosymmetric structures, while $\text{Ag}[(\text{UO}_2)_2\text{B}_5\text{O}_8(\text{OH})_2]$ and $\alpha\text{-Cs}[(\text{UO}_2)_2\text{B}_{11}\text{O}_{16}(\text{OH})_6]$ are centrosymmetric. $\text{Li}[(\text{UO}_2)_2\text{B}_5\text{O}_9] \cdot \text{H}_2\text{O}$, which can be obtained as pure phase, displays second-harmonic generation of 532 nm light from 1064 nm light. Topological relationships of all actinyl borates are developed.

Introduction

Borate materials are being actively developed owing to their wide range of applications. In particular, they display remarkable transparency in the deep UV, high chemical stability, and for some materials, crystals with high optical quality can be obtained leading to the development of nonlinear optical materials when the borates adopt noncentrosymmetric space groups such as $\beta\text{-BaB}_2\text{O}_4$ (**BBO**),¹ LiB_3O_5 (**LBO**),² $\text{CsLiB}_6\text{O}_{10}$ (**CLBO**),³ BiB_3O_6 (**BiBO**),⁴ and $\text{La}_2\text{CaB}_{10}\text{O}_{19}$ (**LCB**).⁵ From a structural chemistry point of view, boron atoms bound by oxygen atoms are found not only in 3-fold (triangle, BO_3) coordination, but also in 4-fold coordination (tetrahedron, BO_4). These BO_3 and BO_4 units can further polymerize to create larger borate clusters by sharing common corners to create clusters, one-dimensional chains, two-dimensional sheets, and three-dimensional framework structures.⁶ Because there is a vast number of different topological arrangements of the polyborate anions, the solid-state and materials chemistry

of borates is virtually unsurpassed.^{6,7} Borates can be divided into three groups: main group and transition metal borates,^{8–13} lanthanide and actinide borates,^{14–28} organic and transition metal complex templated borates.²⁹ Recent

*Address correspondence to either author. E-mail: talbrecl@nd.edu.

- (1) Chen, C.; Wu, B.; Jiang, A.; You, G. *Sci. Sintering* **1984**, *B7*, 598.
(2) Chen, C.; Wu, Y.; Jiang, A.; Wu, B.; You, G.; Li, R.; Lin, S. *J. Opt. Soc. Am. B* **1989**, *6*, 616.
(3) Mori, Y.; Kuroda, I.; Nakajima, S.; Sasaki, T.; Nakai, S. *Appl. Phys. Lett.* **1995**, *67*, 1818.
(4) Hellwig, H.; Liebertz, J.; Bohaty, L. *J. Appl. Phys.* **2000**, *88*, 240.
(5) Wu, Y. C.; Liu, J. G.; Fu, P. Z.; Wang, J. X.; Zhou, H. Y.; Wang, G. F.; Chen, C. T. *Chem. Mater.* **2001**, *13*, 753.
(6) Burns, P. C.; Grice, J. D.; Hawthorne, F. C. *Can. Mineral.* **1995**, *33*, 1131. (b) Grice, J. D.; Burns, P. C.; Hawthorne, F. C. *Can. Mineral.* **1999**, *37*, 731–762.

- (7) (a) Belokoneva, E. L. *Cryst. Res. Technol.* **2008**, *43*, 1173. (b) Yuan, G.; Xue, D. *Acta Crystallogr.* **2007**, *B63*, 353.
(8) (a) Touboul, M.; Penin, N.; Nowogrocki, G. *Solid State Sci.* **2003**, *5*, 1327. (b) Yang, T.; Sun, J.; Li, G.; Wang, Y.; Christensen, J.; He, Z.; Christensen, K. E.; Zou, X.; Liao, F.; Lin, J. *Inorg. Chem.* **2009**, *48*, 11209.
(9) (a) Sevov, S. C. *Angew. Chem., Int. Ed.* **1996**, *35*, 2630. (b) Yang, W.; Li, J.; Pan, Q.; Jin, Z.; Yu, J.; Xu, R. *Chem. Mater.* **2008**, *20*, 4900. (c) Yang, M.; Yu, J.; Di, J.; Li, J.; Chen, P.; Fang, Q.; Chen, Y.; Xu, R. *Inorg. Chem.* **2006**, *45*, 3588. (d) Xing, H.; Li, Y.; Su, T.; Xu, J.; Yang, W.; Zhu, E.; Yu, J.; Xu, R. *Dalton Trans.* **2010**, *39*, 1713. (e) Wang, Y.; Yu, J.; Pan, Q.; Du, Y.; Zou, Y.; Xu, R. *Inorg. Chem.* **2004**, *43*, 559. (f) Yang, G.-Y.; Sevov, S. C. *Inorg. Chem.* **2001**, *40*, 2214. (g) Dumas, E.; Debieuvre-Chouvy, C.; Sevov, S. C. *J. Am. Chem. Soc.* **2002**, *124*, 908. (h) Dumas, E.; Sassoye, C.; Smith, K. D.; Sevov, S. C. *Inorg. Chem.* **2002**, *41*, 4029.
(10) (a) Zhang, H.-X.; Zhang, J.; Zheng, S.-T.; Yang, G.-Y. *Inorg. Chem.* **2005**, *44*, 1166. (b) Lin, Z.-E.; Zhang, J.; Yang, G.-Y. *Inorg. Chem.* **2003**, *42*, 1797. (c) Li, Y.-F.; Zou, X.-D. *Acta Crystallogr.* **2003**, *C59*, 471. (d) Zhang, H.-X.; Zhang, J.; Zheng, S.-T.; Wang, G.-M.; Yang, G.-Y. *Inorg. Chem.* **2004**, *43*, 6148. (e) Wang, G.-M.; Sun, Y.-Q.; Yang, G.-Y. *Cryst. Growth Des.* **2005**, *5*, 313. (f) Xiong, D.-B.; Zhao, J.-T.; Chen, H.-H.; Yang, X.-X. *Chem.—Eur. J.* **2007**, *13*, 9862. (g) Xiong, D.-B.; Chen, H.-H.; Li, M.-R.; Yang, X.-X.; Zhao, J.-T. *Inorg. Chem.* **2006**, *45*, 9301.
(11) (a) Ju, J.; Lin, J.; Li, G.; Yang, T.; Li, H.; Liao, F.; Loong, C.-K.; You, L. *Angew. Chem., Int. Ed.* **2003**, *42*, 5607. (b) Ju, J.; Yang, T.; Li, G.; Liao, F.; Wang, Y.; You, L.; Lin, J. *Chem.—Eur. J.* **2004**, *10*, 3901. (c) Yang, T.; Ju, J.; Li, G.; Liao, F.; Zou, X.; Deng, F.; Chen, L.; Wang, Y.; Lin, J. *Inorg. Chem.* **2007**, *46*, 4772. (d) Rong, C.; Yu, Z.; Wang, Q.; Zheng, S.-T.; Pan, C.-Y.; Deng, F.; Yang, G.-Y. *Inorg. Chem.* **2009**, *48*, 3650. (e) Zhou, J.; Fang, W.-H.; Rong, C.; Yang, G.-Y. *Chem.—Eur. J.* **2010**, *16*, 4852.

interest in borates has focused on mixed oxoanion systems that include B—O—P,⁹ B—O—Ge,¹⁰ B—O—Al,¹¹ B—O—Ga^{11a,12} and B—O—In¹³ systems, with a clear effort to prepare microporous zeolitic materials with new catalytic, ion exchange, and sorption properties.

There are a variety of fruitful methodologies for preparing borate compounds. The most important ones are traditional hydrothermal and solvothermal methods, high-temperature fluxes, and room temperature slow evaporation. Actinide borates are difficult to prepare by traditional hydrothermal methods, because water competes very successfully with borate for inner-sphere coordination sites for these metals under most conditions. In fact, many borates that occur naturally are found in evaporated deposits in arid regions. Actinide borates have been synthesized by either removing water entirely from the system in high-temperature reactions or slow water evaporation. The first single crystal structure of a uranium borate, K₆[UO₂{B₁₆O₂₄(OH)₈}]·12H₂O, was obtained by Behm from crystals obtained from the slow evaporation of water.¹⁵ This compound consists of isolated clusters composed of molecular uranyl borates with a uranyl core surrounded by a 16-borate ring. Shortly after this report Gasperin synthesized seven uranyl borates, including UO₂(B₂O₄), Li(UO₂)BO₃, Na(UO₂)BO₃, Ca(UO₂)₂(BO₃)₂, Mg(UO₂)B₂O₅, Ni₇(UO₂)(B₄O₁₄) and Th(B₂O₅) by using molten B₂O₃ as a flux in high tem-

perature reactions.^{16–22} No new actinide borates were then reported for almost 20 years.

Our strategy for preparing actinide borates is to capitalize on low temperature boric acid flux reactions that have yielded a thorium borate, [ThB₅O₆(OH)₆][BO(OH)₂]·2.5H₂O (**NDTB-1**), with a cationic framework structure and remarkable anion exchange capabilities,²³ a large family of uranyl borates,^{24–27} three mixed-valent neptunium borates,^{24,28} and a single plutonium(VI) borate which is similar to its uranium counterparts.²⁴ We have shown that boric acid fluxes are an excellent medium for preparing actinide borates in general. These conditions yield completely new coordination environments and topologies for actinide compounds.^{23–28} In addition, a significant percentage of uranyl borates adopt noncentrosymmetric structures, and these compounds may aid in the design of nonlinear optical materials. Among the 17 uranyl borates we have already reported, 11 of them adopt noncentrosymmetric space groups.^{24–27} In this report, we substantially expand the uranyl borate family to include compounds that contain lithium, silver, and cesium, completing the series of common monovalent cations. We show that uranyl borates are very sensitive to the cations in the crystal structures, that is, subtle changes in composition can lead to dramatic changes in properties (herein, nonlinear optical properties and fluorescence). Finally, we summarize the topological relationships of the borate networks and general aspects of the synthetic conditions for all the actinide borates we have prepared.

Experimental Section

Syntheses. UO₂(NO₃)₂·6H₂O (98%, International Bio-Analytical Industries), H₃BO₃ (99.99%, Alfa-Aesar), LiNO₃ (99%, Alfa-Aesar), CsNO₃ (99.8%, Alfa-Aesar) and AgNO₃ (99.7%, J. T. Baker) were used as received without further purification. Distilled and Millipore filtered water with resistance of 18.2 MΩ·cm was used in all reactions. PTFE-lined autoclaves were used for all reactions. *While the UO₂(NO₃)₂·6H₂O used in this study contained depleted U, there is really not much compositional difference between depleted uranium and natural abundance uranium, and standard precautions for handling radioactive materials should be followed at all times. There are very old sources of uranyl nitrate that may not be depleted, and enhanced care is warranted for these samples.*

Synthesis of Li[(UO₂)B₅O₉]·H₂O (LiUBO-1). UO₂(NO₃)₂·6H₂O (0.5000 g, 1 mmol), boric acid (0.4944 g, 8 mmol), LiNO₃ (0.0690 g, 4 mmol) and water (50 μL) were loaded into a 23 mL autoclave. The autoclave was sealed and heated to 190 °C in a box furnace for one day. The autoclave was then cooled down to room temperature at a rate of 5 °C/h. The products were washed with boiling water to remove excess boric acid, followed by rinsing with methanol. Crystals in the form of tablets with yellow-green coloration were collected as a pure phase for Li[(UO₂)B₅O₉]·H₂O (**LiUBO-1**) which is confirmed by the powder diffraction of the sample. One day reactions are appropriate for screening product composition, but only lead to low isolated yields. The yield maximizes after three days at 59% based on U.

Synthesis of Ag[(UO₂)B₅O₈(OH)₂] (AgUBO-1). AgUBO-1 can be prepared using UO₂(NO₃)₂·6H₂O, boric acid, AgNO₃ at different Ag:U:B molar ratios of 1:1:8, 1:1:15, 1:1:22, 2:1:8, 2:1:15, 2:1:22, 3:1:15, 3:1:22 by following the similar procedure

- (12) (a) Barbier, J.; Park, H. *Acta Crystallogr.* **2000**, C56, 1057. (b) Li, R. K.; Yu, Y. *Inorg. Chem.* **2006**, 45, 6840. (c) Liu, Z.-H.; Yang, P.; Li, P. *Inorg. Chem.* **2007**, 46, 2965.
- (13) (a) Kononova, N. G.; Kokh, A. E.; Bekker, T. B.; Fedorov, P. P.; Tkachenko, E. A. *Inorg. Mater.* **2004**, 40, 1208. (b) Cox, J. R.; Keszler, D. A. *Acta Crystallogr.* **1994**, C50, 1857. (c) Cong, R.; Yang, T.; Li, H.; Liao, F.; Wang, Y.; Lin, J. *Eur. J. Inorg. Chem.* **2010**, 11, 1703.
- (14) (a) Lu, P.; Wang, Y.; Lin, J.; You, L. *Chem. Commun.* **2001**, 13, 1178. (b) Li, L.; Lu, P.; Wang, Y.; Jin, X.; Li, G.; Wang, Y.; You, L.; Lin, J. *Chem. Mater.* **2002**, 14, 4963. (c) Li, L.; Jin, X.; Li, G.; Wang, Y.; Liao, F.; Yao, G.; Lin, J. *Chem. Mater.* **2003**, 15, 2253. (d) Belokoneva, E. L.; Stefanovich, S. Yu.; Dimitrova, O. V.; Ivanova, A. G. *Zh. Neorg. Khim.* **2002**, 47, 370. (e) Bernadette, S.; Marcus, V.; Claude, F. *J. Solid State Chem.* **1980**, 34, 271.
- (15) Behm, H. *Acta Crystallogr.* **1985**, C41, 642.
- (16) Gasperin, M. *Acta Crystallogr.* **1987**, C43, 1247.
- (17) Gasperin, M. *Acta Crystallogr.* **1987**, C43, 2031.
- (18) Gasperin, M. *Acta Crystallogr.* **1987**, C43, 2264.
- (19) Gasperin, M. *Acta Crystallogr.* **1988**, C44, 415.
- (20) Gasperin, M. *Acta Crystallogr.* **1989**, C45, 981.
- (21) Gasperin, M. *Acta Crystallogr.* **1990**, C46, 372.
- (22) Gasperin, M. *Acta Crystallogr.* **1991**, C47, 10.
- (23) Wang, S.; Alekseev, E. V.; Diwu, J.; Casey, W. H.; Phillips, B. L.; Depmeier, W.; Albrecht-Schmitt, T. E. *Angew. Chem., Int. Ed.* **2010**, 49, 1057.
- (24) Wang, S.; Alekseev, E. V.; Ling, J.; Skanthakumar, S.; Soderholm, L.; Depmeier, W.; Albrecht-Schmitt, T. E. *Angew. Chem., Int. Ed.* **2010**, 49, 1263.
- (25) Wang, S.; Alekseev, E. V.; Ling, J.; Liu, G.; Depmeier, W.; Albrecht-Schmitt, T. E. *Chem. Mater.* **2010**, 22, 2155.
- (26) Wang, S.; Alekseev, E. V.; Stritzinger, J. T.; Depmeier, W.; Albrecht-Schmitt, T. E. *Inorg. Chem.* **2010**, 49, 2948.
- (27) Wang, S.; Alekseev, E. V.; Stritzinger, J. T.; Depmeier, W.; Albrecht-Schmitt, T. E. *Inorg. Chem.* **2010**, 49, 6690.
- (28) Wang, S.; Alekseev, E. V.; Depmeier, W.; Albrecht-Schmitt, T. E. *Chem. Com.* **2010**, 46, 3955.
- (29) (a) Wang, M.-S.; Guo, G.-C.; Chen, W.-T.; Xu, G.; Zhou, W.-W.; Wu, K.-J.; Huang, J.-S. *Angew. Chem., Int. Ed.* **2007**, 46, 3909. (b) Visi, M. Z.; Knobler, C. B.; Owen, J. J.; Khan, M. I.; Schubert, D. M. *Cryst. Growth Des.* **2006**, 6, 538. (c) Yang, S. H.; Li, G. B.; Tian, S. J.; Liao, F. H.; Lin, J. H. *Cryst. Growth Des.* **2007**, 7, 1246. (d) Wang, G.-M.; Sun, Y.-Q.; Yang, G.-Y. *J. Solid State Chem.* **2006**, 179, 1545.

Table 1. Crystallographic Data for Li[UO_2] B_5O_9 · H_2O (LiUBO-1), Ag[(UO_2) $\text{B}_5\text{O}_8(\text{OH})_2$] (AgUBO-1), α -Cs[(UO_2) $_2\text{B}_{11}\text{O}_{16}(\text{OH})_6$] (CsUBO-1), and β -Cs[(UO_2) $_2\text{B}_{11}\text{O}_{16}(\text{OH})_6$] (CsUBO-2)

compound	LiUBO-1	AgUBO-1	CsUBO-1	CsUBO-2
mass	493.04	591.95	1143.88	1143.88
color and habit	yellow-green, tablet	light yellow, tablet	yellow-green, prism	yellow-green, tablet
space group	Pn	$P2_1/n$	$P\bar{1}$	Cc
a (Å)	6.3783(6)	6.4341(6)	6.4069(4)	11.1434(15)
b (Å)	6.2241(5)	12.9804(13)	6.4491(4)	6.4532(9)
c (Å)	10.5308(9)	10.6991(11)	14.0616(8)	27.840(4)
α (deg)	90	90	81.6150(10)	90
β (deg)	90	90.4230(10)	79.4620(10)	96.881(2)
γ (deg)	89.9960(10)	90	60.2390(10)	90
V (Å ³)	418.06(6)	893.53(15)	494.84(5)	1987.6(5)
Z	2	4	1	4
T (K)	293(2)	293(2)	100(2)	100(2)
λ (Å)	0.71073	0.71073	0.71073	0.71073
maximum 2θ (deg.)	28.75	28.75	27.49	28.82
ρ_{calcd} (g cm ⁻³)	3.917	4.400	3.839	3.823
μ (Mo K α)	194.83	203.61	182.88	182.13
$R(F)$ for $F_o^2 > 2\sigma(F_o^2)^a$	0.0267	0.0281	0.0202	0.0385
$Rw(F_o^2)^b$	0.0637	0.0587	0.0505	0.0937

$$^a R(F) = \sum ||F_o| - |F_c|| / \sum |F_o| \quad ^b R(F_o^2) = [\sum w(F_o^2 - F_c^2)^2 / \sum w(F_o^4)]^{1/2}$$

for making the **LiUBO-1**. The reaction duration is three days. Crystals in the form of tablets were isolated from all reactions. The crystals have light yellow coloration. Powder diffraction data from these samples all show **AgUBO-1** as a pure phase in all eight reactions. The highest yield is 65% based on U for the 2:1:15 reaction.

Synthesis of α -Cs[(UO_2) $_2\text{B}_{11}\text{O}_{16}(\text{OH})_6$] (CsUBO-1) and β -Cs[(UO_2) $_2\text{B}_{11}\text{O}_{16}(\text{OH})_6$] (CsUBO-2). CsUBO-1 and CsUBO-2 can be prepared using $\text{UO}_2(\text{NO}_3)_2 \cdot 6\text{H}_2\text{O}$, boric acid, CsNO_3 at different Cs:U:B molar ratios of 3:1:8, 3:1:15 by following the similar procedure for making the **LiUBO-1**. When the reaction duration was three days, **CsUBO-1** and **CsUBO-2** both existed in these two reactions as minor products while β - UB_2O_6 was the major product. When the reaction time was increased to seven days, **CsUBO-1** and **CsUBO-2** both existed in the reaction as the major products while β - UB_2O_6 was the minor product. Crystals were in form of prisms and tablets with yellow-green coloration. The prisms proved to be **CsUBO-1**, while the tablets were **CsUBO-2**.

Crystallographic Studies. Single crystals of all four **LiUBO**, **AgUBO**, and **CsUBO** phases were mounted on glass fibers and optically aligned on a Bruker APEXII CCD X-ray diffractometer or a Bruker APEXII Quazar X-ray diffractometer using a digital camera. Initial intensity measurements were either performed using a $1\mu\text{S}$ X-ray source, a 30 W microfocused sealed tube (MoK α , $\lambda = 0.71073$ Å) with high-brilliance and high-performance focusing Quazar multilayer optics, or a standard sealed tube with a monocapillary collimator. Standard APEXII software was used for determination of the unit cells and data collection control. The intensities of reflections of a sphere were collected by a combination of four sets of exposures (frames). Each set had a different ϕ angle for the crystal and each exposure covered a range of 0.5° in ω . A total of 1464 frames were collected with an exposure time per frame of 10–30 s, depending on the crystal. SAINT was used for data integration including Lorentz and polarization corrections. Semiempirical absorption corrections were applied using the program SADABS. Selected crystallographic data and bond distances information are listed in Tables 1–5. Atomic coordinates and additional structural information are provided in the Supporting Information (CIF's).

Powder X-ray Diffraction. Powder X-ray diffraction patterns of the products of pure **LiUBO** and **AgUBO** reactions were

collected on a Scintag theta–theta diffractometer equipped with a diffracted-beamed monochromatic set for Cu K α ($\lambda = 1.54056$ Å) radiation at room temperature in the angular angle from 10° to 80° (2θ) with a scanning step width of 0.05° and a fixed counting time of 1 s/step. The collected patterns were compared with those calculated from single crystal data using ATOMS.

UV–vis-NIR and Fluorescence Spectroscopy. UV–vis-NIR data were acquired from single crystals of all phases using a Craic Technologies microspectrophotometer. Crystals were placed on quartz slides under Krytox oil, and the data was collected from 200 to 1700 nm. Fluorescence data were obtained using 365 nm light for excitation (see Supporting Information).

Second-Harmonic Generation Measurements. Powder second-harmonic generation (SHG) measurements were performed on a Kurtz-Perry nonlinear optical system.³⁰ A Q-switched Nd:YAG laser (Continuum Surelite I-10), operated at 10 Hz, provided the 1064 nm light used for all measurements. The SHG intensity was recorded from a polycrystalline sample of **LiUBO-1**. No index of refraction matching fluid was used in these experiments. The SHG light at 532 nm was collected in reflection, selected by a narrow band-pass interference filter (Pomfret) and detected by a photomultiplier tube (RCA 1P28). A near normal incidence beam splitter reflected a small fraction of the laser beam onto a pyroelectric detector (Molelectron J3-05) that was used as a laser pulse energy monitor. A digital storage oscilloscope (Tektronix TDS 640A) signal averaged and recorded both the SHG and incident laser energy signals. Average laser power was measured separately with a calibrated Scientech volume absorber calorimeter. *As an important note for other investigators interested in the nonlinear optical properties of radioactive materials: The practice of grinding and sieving powders so that comparisons can be made with reference materials of similar particle size is unsafe. We ground and sieved a less-radioactive thorium compound inside a glovebox and then surveyed the interior of the glovebox. There was a uniform contamination of 50 dpm on every surface tested. We recommend discontinuation of this practice immediately. It is enough to say that there is or is not SHG activity. The magnitude is not important enough to risk the health of researchers.*

(30) Kurtz, S. K.; Perry, T. T. *J. Appl. Phys.* **1968**, *39*, 3798–3813.

Table 2. Selected Bond Distances (Å) for Li[$\text{UO}_2\text{B}_5\text{O}_9$]· H_2O (LiUBO-1)

distance (Å)			
U(1)—O(1)	1.752(5)	B(1)—O(3)	1.331(15)
U(1)—O(2)	1.787(6)	B(1)—O(4)#5	1.399(13)
U(1)—O(6)	2.358(6)	B(1)—O(10)	1.40(2)
U(1)—O(9)#1	2.394(8)	B(2)—O(8)	1.34(2)
U(1)—O(5)	2.426(7)	B(2)—O(7)	1.380(13)
U(1)—O(10)#2	2.478(8)	B(2)—O(11)	1.40(2)
U(1)—O(3)	2.613(8)	B(3)—O(9)	1.403(15)
U(1)—O(4)	2.633(7)	B(3)—O(5)	1.432(15)
		B(3)—O(10)#7	1.439(15)
		B(3)—O(11)#8	1.511(16)
		B(4)—O(7)#9	1.393(11)
		B(4)—O(6)	1.459(11)
		B(4)—O(3)#2	1.506(11)
		B(4)—O(5)#2	1.530(15)
		B(5)—O(4)	1.413(14)
		B(5)—O(9)#2	1.423(15)
		B(5)—O(8)	1.461(14)
		B(5)—O(6)	1.524(14)

Table 3. Selected Bond Distances (Å) for Ag[(UO_2) $\text{B}_5\text{O}_8(\text{OH})_2$] (AgUBO-1)

distance (Å)			
U(1)—O(3)	1.749(5)	B(1)—O(11)	1.453(8)
U(1)—O(5)	1.781(5)	B(1)—O(7)#2	1.464(8)
U(1)—O(7)	2.389(4)	B(1)—O(4)	1.467(9)
U(1)—O(10)	2.397(4)	B(1)—O(9)	1.475(8)
U(1)—O(9)	2.399(5)	B(2)—O(10)	1.458(8)
U(1)—O(8)	2.541(4)	B(2)—O(2)#3	1.464(9)
U(1)—O(12)	2.543(4)	B(2)—O(9)#4	1.466(9)
U(1)—O(11)	2.592(4)	B(2)—O(12)	1.515(8)
		B(3)—O(4)#4	1.361(8)
		B(3)—O(6)	1.361(9)
		B(3)—O(1)	1.376(9)
		B(4)—O(7)	1.452(8)
		B(4)—O(10)#5	1.458(8)
		B(4)—O(6)#5	1.467(8)
		B(4)—O(8)	1.471(8)
		B(5)—O(12)#2	1.345(8)
		B(5)—O(8)#6	1.368(8)
		B(5)—O(11)	1.377(8)

Results and Discussion

Some Aspects of Actinyl Borate Syntheses. There are many factors that control the boric acid flux syntheses of uranyl borates. First, the stoichiometry of the starting materials controls the number of products in the reaction. Small changes in stoichiometry can give rise to substantially different products. The phase diagrams and syntheses tables for all uranyl borates are provided in the Supporting Information, and these data show that each cation behaves differently. Compared to most other ligand systems,³¹ the uranyl borate system is much more sensitive to changes in the size of the cations, and there are few isostructural compounds that exist if the cation is changed (only **RbUBO-2** and **KUBO-3**).²⁷ In the LiUBO system, **LiUBO-1** can only be made in a narrow range of stoichiometries. For the NaUBO and KUBO systems, each of the different stoichiometries tested yields new NaUBO and KUBO phases. For the NaUBO system, low Na:U ratio reactions give a larger number of phases, and the product with higher Na:U

Table 4. Selected Bond Distances (Å) for α -Cs[(UO_2) $\text{B}_{11}\text{O}_{16}(\text{OH})_6$] (CsUBO-1)

distance (Å)			
U(1)—O(5)	1.765(3)	B(1)—O(4)#4	1.357(6)
U(1)—O(9)	1.771(3)	B(1)—O(3)	1.368(6)
U(1)—O(6)	2.385(3)	B(1)—O(1)	1.382(6)
U(1)—O(8)	2.399(2)	B(2)—O(7)#1	1.359(5)
U(1)—O(11)	2.417(3)	B(2)—O(12)#6	1.363(5)
U(1)—O(10)	2.537(3)	B(2)—O(10)	1.373(5)
U(1)—O(12)	2.578(3)	B(3)—O(11)#4	1.452(5)
U(1)—O(7)	2.579(2)	B(3)—O(6)	1.457(5)
		B(3)—O(12)	1.485(5)
		B(3)—O(2)	1.493(5)
		B(4)—O(4)	1.457(5)
		B(4)—O(8)#7	1.462(5)
		B(4)—O(7)	1.466(5)
		B(4)—O(11)	1.494(5)
		B(5)—O(6)	1.455(5)
		B(5)—O(3)	1.466(5)
		B(5)—O(10)#8	1.468(5)
		B(5)—O(8)#8	1.473(5)

Table 5. Selected Bond Distances (Å) for β -Cs[(UO_2) $\text{B}_{11}\text{O}_{16}(\text{OH})_6$] (CsUBO-2)

distance (Å)			
U(1)—O(18)	1.746(9)	B(1)—O(1)	1.436(15)
U(1)—O(15)	1.763(9)	B(1)—O(11)#6	1.453(14)
U(1)—O(14)	2.402(8)	B(1)—O(9)#6	1.480(14)
U(1)—O(7)	2.405(7)	B(1)—O(12)	1.497(14)
U(1)—O(5)	2.416(7)	B(2)—O(5)	1.440(15)
U(1)—O(3)	2.543(8)	B(2)—O(14)#5	1.469(15)
U(1)—O(10)	2.568(7)	B(2)—O(23)	1.492(15)
U(1)—O(21)	2.582(7)	B(2)—O(10)#5	1.501(15)
U(2)—O(17)	1.762(9)	B(3)—O(8)#2	1.442(13)
U(2)—O(16)	1.767(8)	B(3)—O(22)#2	1.443(15)
U(2)—O(11)	2.386(7)	B(3)—O(2)#2	1.480(13)
U(2)—O(1)	2.426(8)	B(3)—O(1)	1.497(14)
U(2)—O(2)	2.430(8)	B(4)—O(11)#3	1.437(14)
U(2)—O(4)	2.552(7)	B(4)—O(2)	1.449(14)
U(2)—O(12)	2.573(7)	B(4)—O(24)	1.475(14)
U(2)—O(22)	2.579(7)	B(4)—O(4)#3	1.510(13)
		B(5)—O(21)#1	1.323(13)
		B(5)—O(10)#5	1.366(13)
		B(5)—O(3)	1.412(13)
		B(6)—O(20)	1.346(16)
		B(6)—O(8)	1.374(15)
		B(6)—O(9)#3	1.395(15)
		B(7)—O(6)	1.334(16)
		B(7)—O(13)#5	1.371(17)
		B(7)—O(19)	1.421(18)
		B(8)—O(7)	1.430(13)
		B(8)—O(21)#4	1.477(14)
		B(8)—O(6)#4	1.483(13)
		B(8)—O(5)#4	1.510(12)
		B(9)—O(12)	1.300(13)
		B(9)—O(4)#3	1.381(13)
		B(9)—O(22)#6	1.407(14)
		B(10)—O(13)	1.430(13)
		B(10)—O(14)	1.437(13)
		B(10)—O(3)#6	1.473(14)
		B(10)—O(7)#6	1.500(14)

ratio can be made pure in higher Na:U ratio reactions.²⁵ In contrast the KUBO system is more complicated. Products with lower K:U ratios can be made pure in lower K:U reactions, while products with higher K:U ratio can be made pure in higher K:U ratio reactions, between these extremes, there are always mixtures of products.²⁷ For the RbUBO and CsUBO systems, which are very similar to the LiUBO system, the products can only be made in a narrow range of stoichiometry. For the AgUBO system, each of the

(31) (a) Almond, P. M.; Albrecht-Schmitt, T. E. *Inorg. Chem.* **2002**, *41*, 1177. (b) Sullens, T. A.; Jensen, R. A.; Shvareva, T. Y.; Albrecht-Schmitt, T. E. *J. Am. Chem. Soc.* **2004**, *126*, 2676.

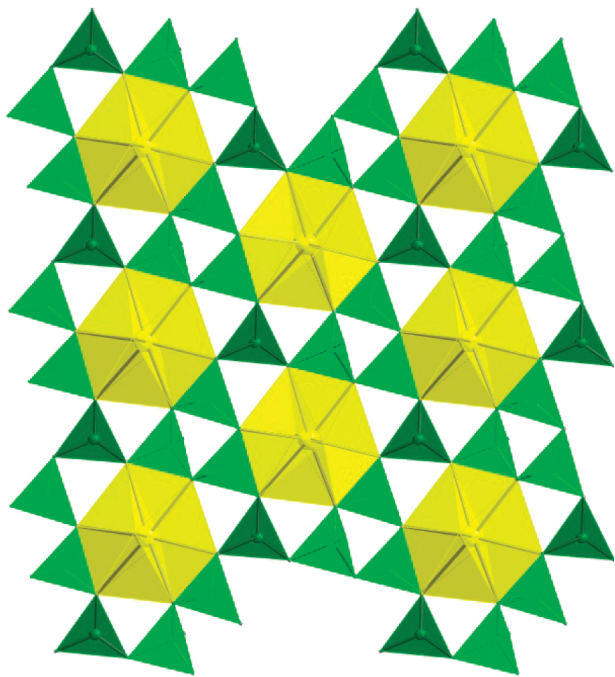


Figure 1. Depiction of local structure of uranyl borate sheets in all compounds. (UO_8 hexagonal bipyramids are shown in yellow, BO_3 triangles in dark green, and BO_4 tetrahedra in light green).

different stoichiometries tested yields only one pure product. For TIUBO system, which is the most complicated we have studied, each of the different stoichiometries tested yields different numbers of products. Only high B:U ratio reactions can give a pure product, **TIUBO-2**.²⁵

All these results are based on short reaction times (24 h), but the reaction duration is another important factor in the preparation of uranyl borates. Longer reactions lead to higher yields, and in some cases also change the number of products. For example, for the Li, Rb, and Cs systems, reaction stoichiometries that do not give rise to desired products in 24 h do eventually yield new products if the heating is prolonged for several more days.

Crystal Structures and Topological Aspects. The structures of the four compounds described in this work are based on similar uranyl borate motifs. The polyborate sheets are based on both BO_4 tetrahedra and BO_3 triangles. These sheets incorporate linear uranyl groups, UO_2^{2+} . As the result of such incorporation the uranium atoms have hexagonal bipyramidal coordination, UO_8 . This coordination is relatively rare in U(VI) chemistry (85% of uranyl compounds contain pentagonal bipyramidal coordination), but all uranyl borates synthesized from molten boric acid contain this type of uranium coordination.^{24–28} This coordination generally requires small chelating ligands, and the borate anions serve this purpose well. Each UO_8 unit is surrounded by three BO_3 triangles and six BO_4 tetrahedra in the sheets showed in Figure 1. Between the polyborate sheets are cations of alkali elements and BO_3 triangles (Figure 2). The dramatic differences between these compounds are realized in the interlayer space rather than in the uranyl borate sheets. The phases can be separated into two groups based on the topological features: 1, $\text{Li}[(\text{UO}_2)\text{B}_5\text{O}_9] \cdot \text{H}_2\text{O}$ (**LiUBO-1**)

and $\text{Ag}[(\text{UO}_2)\text{B}_5\text{O}_8(\text{OH})_2]$ (**AgUBO-1**); 2, $\alpha\text{-Cs}[(\text{UO}_2)_2\text{B}_{11}\text{O}_{16}(\text{OH})_6]$ (**CsUBO-1**) and $\beta\text{-Cs}[(\text{UO}_2)_2\text{B}_{11}\text{O}_{16}(\text{OH})_6]$ (**CsUBO-2**). We will consider the structural features of these phases in more detail.

LiUBO-1 and AgUBO-1. The crystal structure fragments of Li and Ag uranyl borates are shown in Figure 2a and b, respectively. The structure of **LiUBO-1** is a 3D framework based on polyborates sheets linked by BO_3 triangles. The topology of these sheets was previously found only in the structure of $\text{Rb}_2[(\text{UO}_2)_2\text{B}_{13}\text{O}_{20}(\text{OH})_5]$,²⁷ and we named these sheets as **G-type**. The sheets are strongly corrugated along the *c* axis. A similar sheet distortion was observed in the structure of the pure uranyl borate $(\text{UO}_2)_2[\text{B}_{13}\text{O}_{20}(\text{OH})_3] \cdot 1.25\text{H}_2\text{O}$.²⁶ The unit cell of **LiUBO-1** contains only one uranyl borate sheet, and all of them in this structure are in identical positions. The BO_3 linkers interconnect the borate sheets leading to the formation of open cages. Lithium cations are located between two neighboring BO_3 triangles, and have the contacts with oxygen atoms from uranyl groups, polyborate net, and water molecules. The resulting coordination of lithium atoms can be described as a distorted tetragonal pyramid. The water molecules are in open cages and strongly bonded with lithium (1.94 Å) and with oxygen atoms from borate network.

The structure of **AgUBO-1** is based on 2D layers. These layers consist of borate sheets with a topology identical with the sheet topology in **LiUBO-1** (**G-type**), and flat BO_3 triangles are directed perpendicular to the plane of the sheets (Figure 2b). The neighboring layers in the structure are rotated 180° with respect to each other. Ag^+ cations link the uranyl borate layers into a regular 3D structure. The oxygen environment of the Ag^+ cations is a deformed tetrahedron with bond lengths from 2.31 Å to 2.50 Å. It is interesting that in the $\text{Ag}^+ - \text{UO}_2^{2+} - \text{H}_3\text{BO}_3$ system that only one phase forms, whereas in $\text{Na}^+ - \text{UO}_2^{2+} - \text{H}_3\text{BO}_3$ system four phases with a different topology of polyborate sheets was observed.²⁵ Usually silver and sodium uranyl compounds demonstrate a high level of similarity.³²

The relationship between the two structure types is schematically presented in Figure 3. The skeletal representations of the Ag and Li structure types have been plotted in this figure. Here are shown only 2D and 3D borate nets without UO_8 polyhedra, alkali atoms, and water molecules (for Li structure) are shown. In order to transform the structures from the Ag-type to Li-type, we need to turn each second layer by 180° in the plane of the sheets (shown by red dashed arrow), and shift these layers by $1/2$ of *x* and $1/3$ of *z* translations. As a result of these manipulations the BO_2OH triangles (shown in red) will occupy positions very close to BO_3OH tetrahedra (shown in red). The condensation of these groups with concomitant water formation links the layers and yields a 3D structure. The resulting structure has free space within open cages for all water molecules that are formed as is

(32) Alekseev, E. V.; Krivovichev, S. V.; Depmeier, W. *J. Mater. Chem.* **2009**, *19*, 2583.

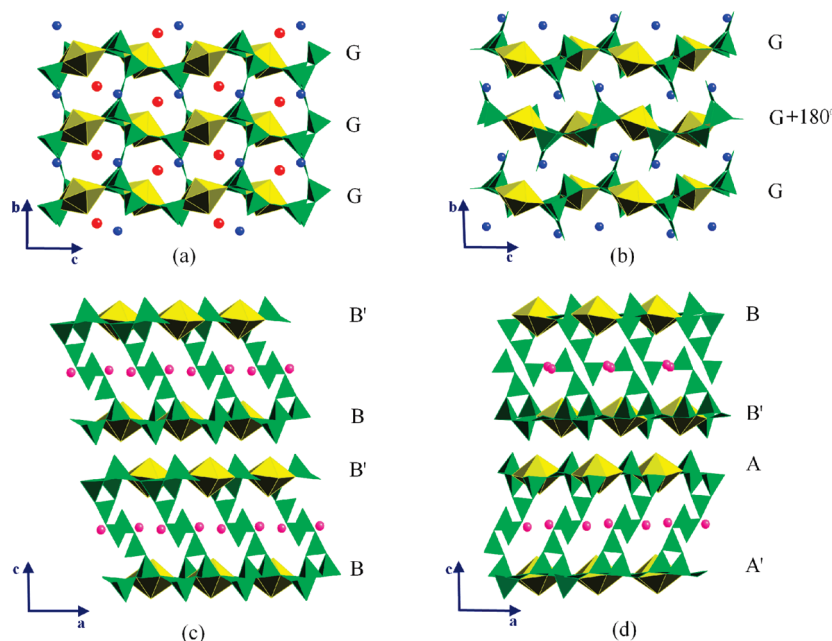


Figure 2. The crystals structures of $\text{Li}[(\text{UO}_2)\text{B}_5\text{O}_9]\cdot\text{H}_2\text{O}$ (a), $\text{Ag}[(\text{UO}_2)\text{B}_5\text{O}_8(\text{OH})_2]$ (b), $\alpha\text{-Cs}[(\text{UO}_2)_2\text{B}_{11}\text{O}_{16}(\text{OH})_6]$ (c), $\beta\text{-Cs}[(\text{UO}_2)_2\text{B}_{11}\text{O}_{16}(\text{OH})_6]$ (d). UO_8 hexagonal bipyramids are shown in yellow, BO_3 and BO_4 units in green, Li and Ag cations in blue, Cs cations in pink, and water molecules in red.

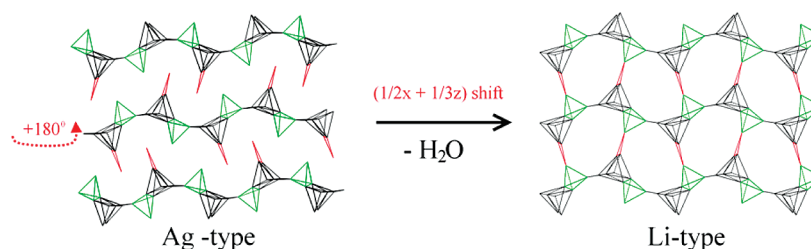


Figure 3. Schematic representation of **LiUBO-1** and **AgUBO-1** structure type relationships.

found in **LiUBO-1**. It is possible that the structure formation of **LiUBO-1** was followed in this way through layered precursors, which is typical for zeolites-like structures.³³


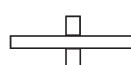
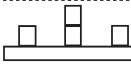
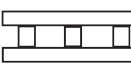
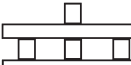

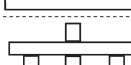
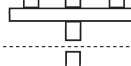
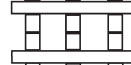



CsUBO-1 and CsUBO-2. The Cs^+ -containing structures have same chemical compositions and very similar crystal structures (Figure 2c,d). They are based on single asymmetrical 2D layers composed of BO_4 tetrahedra, BO_3 triangles, and UO_8 hexagonal bipyramids. These layers can be separated into borate sheets and teeth-like fragments. These fragments are practically perpendicular to the sheet's plane and consist of two BO_3 triangles with a B_2O_5 stoichiometry. The terminal BO_3 triangles in each B_2O_5 group are disordered over two sites with equal occupancy. The reason for this effect is the splitting of the Cs atom positions that appear because of large size of free space between uranyl borate layers. The distance between cesium atoms positions is only ~ 2.19 Å, and these positions are each half occupied. As the results of such splitting the real structures of **CsUBO-1** and **CsUBO-2** based on both BO_3 and B_2O_5 groups simultaneously presented in the interlayer space, because if

the cesium atom settled in nearest position to B_2O_5 group this group should not have a terminal BO_3 triangle. Cs^+ cations link the two uranyl borate layers into quasi double layers. Because of the layer asymmetry the nature of bonding on the different sides of these layers is different. If Cs^+ cations provide mainly ionic bonds ($\text{Cs}-\text{O}$) on the other side of the layers strong hydrogen bonds are observed ($\text{O}-\text{O}$ distances ~ 2.43 Å). In structures of **CsUBO-1** and **CsUBO-2** are logical continuations of $\alpha\text{-Na}[(\text{UO}_2)_2\text{B}_{10}\text{O}_{15}(\text{OH})_5]$ and $\beta\text{-Na}[(\text{UO}_2)_2\text{B}_{10}\text{O}_{15}(\text{OH})_5]$ structure types evolution.²⁵ The cesium structures adopt additional space (this space appears because of the increase in size of the interlayer cations) with the addition of BO_3 groups and formation of teeth-like fragments.

The topology of the borate sheets in **CsUBO-1** and **CsUBO-2** are the same with A/B topology types we found in structures of several borates.^{24–27} The main difference between α - and β - $\text{Cs}[(\text{UO}_2)_2\text{B}_{11}\text{O}_{16}(\text{OH})_6]$ is in topologies alternation. In Figure 2c we can see sheets packed in the structure of α modification. It contains only B and B' type sheets which regularly alternate, **B/B'/B/B'**. The β modification consists from both A and B type sheets (Figure 2d). These types are combined within quasi doubled layers, **B/B'/A/A'**. Such differences in topology and packing provide the unit cell doubling along of

(33) (a) Oberhagemann, U.; Bayat, P.; Marler, B.; Gies, H.; Rius, J. *Angew. Chem., Int. Ed.* **1997**, 35, 2869. (b) Li, Z.; Marler, B.; Gies, H. *Chem. Mater.* **2008**, 20, 1896.

Table 6. High-Level Topology in Actinyl Borates

	Type	Descriptor	Compounds
1		1L-1-0-0	$\alpha\text{-Na}[(\text{UO}_2)_2\text{B}_{10}\text{O}_{15}(\text{OH})_5]^{25}$ $\beta\text{-Na}[(\text{UO}_2)_2\text{B}_{10}\text{O}_{15}(\text{OH})_5]^{25}$ $\text{Na}[(\text{UO}_2)_2\text{B}_{10}\text{O}_{15}(\text{OH})_5] \cdot 3\text{H}_2\text{O}^{25}$ $\text{K}[(\text{UO}_2)_2\text{B}_{10}\text{O}_{15}(\text{OH})_5]^{27}$
2		1L-1-1-0	$\text{Ag}[(\text{UO}_2)_2\text{B}_5\text{O}_8(\text{OH})_2]^{25}$ $\alpha\text{-Tl}_2[(\text{UO}_2)_2\text{B}_{11}\text{O}_{18}(\text{OH})_3]^{25}$ $\text{K}_4(\text{NpO}_2)_{6.73}[\text{B}_{20}\text{O}_{36}(\text{OH})_2] [2\text{L}-1-1-0]_{2\text{Np}}^{24}$ $\text{Ba}_2(\text{NpO}_2)_{6.59}[\text{B}_{20}\text{O}_{36}(\text{OH})_2] \cdot \text{H}_2\text{O} [2\text{L}-1-1-0]_{2\text{Np}}^{24}$ $\text{K}_2[(\text{NpO}_2)_3\text{B}_{10}\text{O}_{16}(\text{OH})_2(\text{NO}_3)_2] [2\text{L}-1-1-0]_{\infty\text{Np}}^{28}$
3		1L-2/1-0-0	$\alpha\text{-Cs}[(\text{UO}_2)_2\text{B}_{11}\text{O}_{15}(\text{OH})_5]^{25}$ $\beta\text{-Cs}[(\text{UO}_2)_2\text{B}_{11}\text{O}_{15}(\text{OH})_5]^{25}$
4		2L-0-0-1	$\alpha\text{-(UO}_2)_2[\text{B}_9\text{O}_{14}(\text{OH})_4]^{26}$ $\beta\text{-(UO}_2)_2[\text{B}_9\text{O}_{14}(\text{OH})_4]^{26}$ $\gamma\text{-(UO}_2)_2[\text{B}_9\text{O}_{14}(\text{OH})_4]^{26}$
5		2L-1-1-1	$\beta\text{-Tl}_2[(\text{UO}_2)_2\text{B}_{11}\text{O}_{18}(\text{OH})_3]^{25}$
6		2L-0-0-2	$\text{K}[(\text{UO}_2)_2\text{B}_{10}\text{O}_{16}(\text{OH})_3] \cdot \text{H}_2\text{O}^{27}$ $\text{Rb}[(\text{UO}_2)_2\text{B}_{10}\text{O}_{16}(\text{OH})_3] \cdot 0.7\text{H}_2\text{O}^{27}$ $\text{Tl}[(\text{UO}_2)_2\text{B}_{10}\text{O}_{16}(\text{OH})_3] \cdot \text{H}_2\text{O}^{25}$
7		2L-1-1-2	$\text{K}_2[(\text{UO}_2)_2\text{B}_{12}\text{O}_{19}(\text{OH})_4] \cdot 0.3\text{H}_2\text{O}^{27}$
8		2L-2/1-2/1-2	$\text{Rb}_2[(\text{UO}_2)_2\text{B}_{13}\text{O}_{20}(\text{OH})_5]^{27}$
9		2L-1-1-3	$(\text{UO}_2)_2[\text{B}_{13}\text{O}_{20}(\text{OH})_3] \cdot 1.25\text{H}_2\text{O}^{26}$
10		F-1-1	$\text{Li}[(\text{UO}_2)_2\text{B}_5\text{O}_9] \cdot \text{H}_2\text{O}$
11		F-2-1	$\text{Tl}_2[(\text{UO}_2)_2\text{B}_{11}\text{O}_{19}(\text{OH})]^{25}$
12		F-2-2	$\text{Na}[(\text{UO}_2)_2\text{B}_6\text{O}_{10}(\text{OH})] \cdot 2\text{H}_2\text{O}^{25}$ $\text{PuO}_2[\text{B}_8\text{O}_{11}(\text{OH})_4]^{24}$

c direction and orientation of content within quasi double layers (Cs atoms position and teeth-like fragments, Figure 2d). The addition of the A type layers to the centrosymmetric ($P\bar{1}$) structure of $\alpha\text{-Cs}[(\text{UO}_2)_2\text{B}_{11}\text{O}_{16}(\text{OH})_6]$ makes the new structure of $\beta\text{-Cs}[(\text{UO}_2)_2\text{B}_{11}\text{O}_{16}(\text{OH})_6]$ noncentrosymmetric (Cc). We have previously observed this in several uranyl borates.^{24–27}

Some Aspects of Actinyl Borate Topologies. We have thus far reported 25 actinide borates including those in this paper.^{23–28} All of these compounds contain linear actinyl groups ($\text{O}=\text{An}=\text{O}$) contained within borate sheets except for $\text{Th}[\text{B}_5\text{O}_6(\text{OH})_6] [\text{BO}(\text{OH})_2] \cdot 2.5\text{H}_2\text{O}$

(NDTB-1).²³ The borate sheets play the role of a matrix which incorporates linear actinyl groups in triangular pores. Our recent results demonstrate that such borate sheets can have different types of topologies because of complicated ordering of BO_3 and BO_4 groups within them. This level of topology could be described as a “fine topology” (detailed topology within finite clusters). But as we demonstrated in our previous works borate sheets can be modified by the addition of BO_3 and BO_4 fragments directed perpendicular to the sheets plane. The result of such modification is several types of structural motifs in actinyl borates: single layers, doubled layers,

and 3D frameworks where BO_3 and BO_4 play the role of 2D sheet linkers. This feature makes groups of actinide borates unique in all of actinide chemistry. Here we would like to systemize the hierarchy of the structural motifs in actinyl borates based on sheets.

The simplest actinyl structures based on layers are constructed from polyborate sheet with one additional BO_3 triangular group. Schematically this structure type is shown in left side of first line in Table 6. These layers are asymmetric and have different types of bonding on different sides, ionic with cations from side where triangles are, and strong hydrogen bonds on the opposite side. To describe these layers in the form of simple record we use descriptor **1 L-1-0-0** where **1 L-** means single layer, **1-0-0** demonstrates the number of additional BO_3 and/or BO_4 groups up/down on the layers (first two digits), and number of intersheet linkers in the case if structure based on double layers (for single layers it is 0, if double layers linked via one boron based groups its is 1 and etc. up to 3). If we add the one additional BO_3 group to make layers symmetrical we will have **1 L-1-1-0** type, which is shown in the second row. These phases are quite different, but are all based on similar 2D polyborate sheets with symmetrical perpendicular BO_3 groups. In the structures of neptunium phases **1 L-1-1-0** single layers are linked via cation-cation interactions of neptunyl groups into double layers, and a 3D framework.^{24,28} The biggest cations require more space, and yield the possibility of **1 L-2/1-0-0** single layer formation in Cs uranyl borates (**2/1-** is an alternation of BO_3 and B_2O_5 groups). The simplest double layers in reviewing these groups have the **2 L-0-0-1** descriptor, and are shown in row four of Table 6. These layers are realized only in simplest modifications of pure uranyl borates (three forms: α , β , and γ). The other layers are formed with additional BO_3 and/or BO_4 groups in the external and internal positions. The double layers in actinyl borates can have from one to two BO_3 groups in external positions, and from one to three BO_3 and/or BO_4 groups as linkers (internal positions). The complexity of the phases based on double layers increases with increasing of the U/B ratios. This is obvious from Table 6. The U/B ratio in the simplest phases with double layers is less than in all others: 1/4.5 (row 6). When the ratio increased to 1/6.5 we have very complicate phases based on double layers with B_2O_5 and B_3O_7 linkers and BO_3 and B_2O_5 external groups (rows 8 and 9). It is interesting that structural complexity is not dependent on monovalent metal cation sizes.

For describing frameworks based on 2D sheets we used similar descriptors. In these descriptors the first letter has been changed from **L** to **F** (framework) and last digit was eliminated because frameworks do not have external positions (all are internal). The simplest framework realized in the discussed above is the Li uranyl borate. In this structure 2D borate sheets are linked by single BO_3 groups and the descriptor is **F-1-1**. If one BO_3 group is added from only one side the **F-2-1** structure is realized. Such a structure type was found in $\text{Th}_2[(\text{UO}_2)_2\text{B}_{11}\text{O}_{19}(\text{OH})]$ (row 11). The symmetric framework with **F-2-2** descriptor was realized

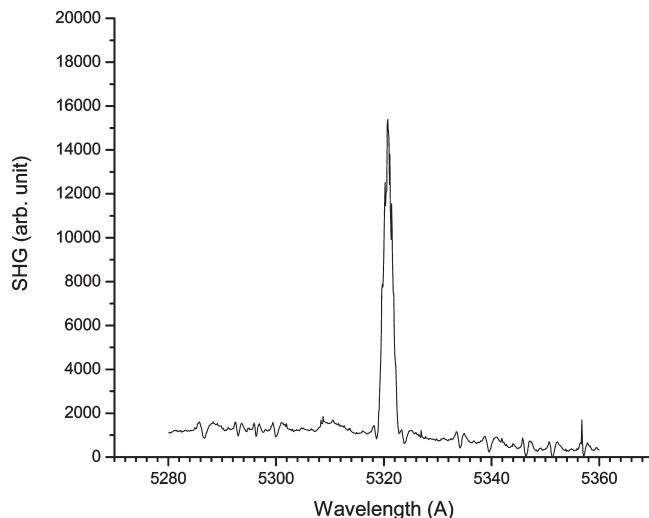


Figure 4. Second-harmonic generation of 532 nm laser light from 1064 nm laser light getting from a polycrystalline sample of **LiUBO-1**.

in $\text{Na}[(\text{UO}_2)_2\text{B}_6\text{O}_{10}(\text{OH})] \cdot 2\text{H}_2\text{O}$ and $\text{PuO}_2[\text{B}_8\text{O}_{11}(\text{OH})_4]$ where the last phase demonstrated largest ratio An/B-1/8 .

The approach to high-level topology presentation described above is easily modified and can be applied to various actinyl phases which have similar structural features.

Nonlinear Optical Properties. **LiUBO-1** crystallizes in the noncentrosymmetric space group Pn , and can be obtained as a pure phase. This space group is also polar, and this being the case the compound is capable of exhibiting a wide range of physical properties include the second-harmonic generation of light when irradiated with a laser. Indeed when a polycrystalline sample of **LiUBO-1** is irradiated with 1064 nm light, 532 light is clearly observed as shown in Figure 4.

Fluorescence Properties. The term “fluorescence” was created in the 18th century to describe the green glow from uranyl salts that occurs when natural light irradiates them. This emission is in fact highly complex and is strongly vibronically coupled charge-transfer emission. Emission from uranyl compounds has been carefully and extensively studied, especially by Denning and co-workers who assigned all of the vibronic transitions from single crystals containing the $[\text{UO}_2\text{Cl}_4]^{2-}$ anion.³⁴ While five broad features centered near 520 nm are generally observed for uranyl compounds at room temperature, far more bands are resolved at low temperatures.

$\text{Li}[(\text{UO}_2)_2\text{B}_5\text{O}_9] \cdot \text{H}_2\text{O}$ (**LiUBO-1**), $\alpha\text{-Cs}[(\text{UO}_2)_2\text{B}_{11}\text{O}_{16}(\text{OH})_6]$ (**CsUBO-1**), and $\beta\text{-Cs}[(\text{UO}_2)_2\text{B}_{11}\text{O}_{16}(\text{OH})_6]$ (**CsUBO-2**) all form crystals with the pale yellow-green coloration. Upon irradiation with 365 nm light, these crystals fluoresce with sufficient intensity that the emission from a few crystals is easily observed by the naked eye. The fluorescence spectra are all provided in the Supporting Information, and given that all of the uranyl borates contain very similar site symmetry around the uranium atoms (D_{6h}), it is not surprising that there are little differences

(34) Denning, R. G.; Norris, J. O. W.; Short, I. G.; Snellgrove, T. R.; Woodwark, D. R. *Lanthanide and Actinide Chemistry and Spectroscopy*, ACS Symp. Ser. No. 131; Edelman, N. M., Ed; American Chemical Society: Washington, DC, 1980; Chapter 15.

among these data. However, $\text{Ag}[(\text{UO}_2)\text{B}_5\text{O}_8(\text{OH})_2]$ (**AgUBO-1**) forms crystals with light yellow coloration, and these crystals do not show any fluorescence signal upon the 365 nm irradiation. It is expected that the Ag^+ quenches the fluorescence feature from the uranyl units. Thallium also quenches the fluorescence in all of the thallium uranyl borates.

Conclusions

Our original interest in actinide borates stemmed from their potential formation in vitrified nuclear waste, and in fact, some of these phases are of sufficient thermal stability that they might form in molten borosilicate glasses.^{24,25} Such compounds may also be produced as vitrified waste is altered on a geologic time-scale in a nuclear waste repository. However, it became immediately clear on a more fundamental level that actinide borates were structurally unique among actinide oxoanion families. The complexity of the polyborate sheets and frameworks is unparalleled, and of equal importance the family is dominated by the formation of acentric structures. We have developed syntheses that lead to the formation of pure crystalline phases, and these compounds show nonlinear optical properties, and most of them also fluoresce. While we think it is unlikely uranyl borates will be used as nonlinear optical materials, the principles learned about the structures of these materials

may instruct us in how to prepare nonradioactive analogs that are truly useful in this application. This report completes the series of uranyl borates with common monovalent cations, and we have developed a simple graphical representation for organizing these complex materials.

Acknowledgment. We are grateful for support provided by the Chemical Sciences, Geosciences, and Biosciences Division, Office of Basic Energy Sciences, Office of Science, Heavy Elements Program, U.S. Department of Energy, under Grant DE-FG02-01ER16026 and DE-SC0002215, and by Deutsche Forschungsgemeinschaft for support within the DE 412/30-2 research project. This material is based upon work supported as part of the Materials Science of Actinides, an Energy Frontier Research Center funded by the U.S. Department of Energy, Office of Science, Office of Basic Energy Sciences under Award Number DE-SC0001089. The National Science Foundation also supported a portion of this work through the REU program in solid-state and materials chemistry (DMR).

Supporting Information Available: X-ray crystallographic files for $\text{Li}[(\text{UO}_2)\text{B}_5\text{O}_9] \cdot \text{H}_2\text{O}$ (**LiUBO-1**), $\text{Ag}[(\text{UO}_2)\text{B}_5\text{O}_8(\text{OH})_2]$ (**AgUBO-1**), $\alpha\text{-Cs}[(\text{UO}_2)_2\text{B}_{11}\text{O}_{16}(\text{OH})_6]$ (**CsUBO-1**), $\beta\text{-Cs}[(\text{UO}_2)_2\text{B}_{11}\text{O}_{16}(\text{OH})_6]$ (**CsUBO-2**). Fluorescence data, phase diagrams, and product compositions are also provided here. This material is available free of charge via the Internet at <http://pubs.acs.org>.